chemengineering

MDPI

Review

Recent Advances in the Preparation of Barium Sulfate Nanoparticles: A Mini-Review

Tlek Ketegenov [1], Kaster Kamunur [1,2], Aisulu Batkal [1], Diana Gani [1] and Rashid Nadirov [1,2,*]

[1] Institute of Combustion Problems, Laboratory of Mechanochemical Processes and Combustion Problems, Almaty 050012, Kazakhstan; tlek58@mail.ru (T.K.); kamunur.k@mail.ru (K.K.); abatkalova@mail.ru (A.B.); dianka777@yahoo.co.uk (D.G.)

[2] Department of General and Inorganic Chemistry, Al-Farabi Kazakh National University, Almaty 050040, Kazakhstan

* Correspondence: nadirov.rashid@gmail.com; Tel.: +7-747-452-05-25

Abstract: The potential for barium sulphate nanoparticles to be used in a variety of important fields has sparked a lot of attention. Methods for obtaining this material by milling (top-down approach) are not very popular due to the difficulty of controlling the size and shape of particles, as well as changes in their physicochemical properties during milling. More promising is the bottom-up approach, which is the interaction of Ba^{2+} and SO_4^{2-} ions in a liquid environment. Direct precipitation is the simplest method; however, it does not allow control of the particle size. Microemulsions, microreactors membrane dispersion, as well as spinning disc reactors are used to overcome drawbacks of direct precipitation and allow control of particle size and shape. This is ensured mainly by intensive controlled micromixing of the precursors with concentrations close to saturated ones. The present review focuses on recent advances in the production of barium sulfate nanoparticles using various approaches, as well as their advantages and limitations. The issues of scaling up the techniques are also considered, and promising methods for obtaining $BaSO_4$ nanoparticles are also discussed.

Keywords: barium sulfate; nanoparticle obtaining; top-down; bottom-up; particle size

Citation: Ketegenov, T.; Kamunur, K.; Batkal, A.; Gani, D.; Nadirov, R. Recent Advances in the Preparation of Barium Sulfate Nanoparticles: A Mini-Review. *ChemEngineering* **2022**, *6*, 30. https://doi.org/10.3390/chemengineering6020030

Academic Editor: Jacek B. Jasinski

Received: 18 March 2022
Accepted: 12 April 2022
Published: 14 April 2022

1. Introduction

Nanoparticles (NPs) are commonly referred to as solid-phase objects which have at least one dimension less than 100 nm. The small size of nanoparticles gives them unusual structural, optical, electronic, magnetic and chemical properties [1–4]. This circumstance determines the wide application of nanoparticles in such areas as pharmaceuticals, fine chemicals, cosmetics, food, ceramics, catalysts, electronics, pigments, and other industries [5–11].

One of the NPs of great industrial importance is barium sulfate ($BaSO_4$). Barium sulfate is a salt composed of the barium cation (Ba^{2+}) and the sulfate anion (SO_4^{2-}), in which sulfur is attached to four oxygen atoms (Figure 1).

Being an NP, this inorganic material is primarily used in the filling materials and additives of paper, paints, plastics, pigments, cosmetics, ceramics, and orthopedics among others [12–18]. It has also been reported that the incorporation of $BaSO_4$ NPs into polyurethane elastomer pellethane enhanced its antimicrobial properties in vitro toward some bacteria causing disease in plants, animals and humans [19,20]. Besides, barium sulfate NPs outperform microscale $BaSO_4$ particles, which are currently used as an X-ray contrast agent in medicine [21]. Nowadays, the production of $BaSO_4$ NPs with well-defined properties of the resulting particle size distribution (PSD) by simple and powerful methods is still challenging. The following problems must be addressed when obtaining this product. First, it is necessary to ensure the stability of the system with giant surface energy, since NPs have a very large interface. Secondly, it is often required to obtain NPs with the desired morphology including the required crystal size, narrow particle size distribution, and the

required microstructure. Further, it is necessary to ensure the resistance of NPs to unwanted agglomeration or sticking after the end of the synthesis.

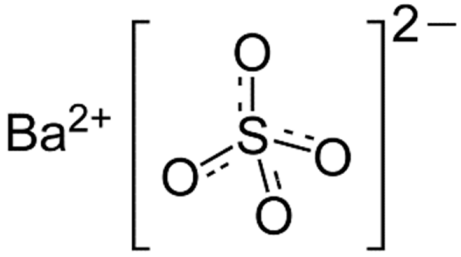

Figure 1. Chemical structure of barium sulfate.

Typically, there are two general strategies to obtain NPs. One is the top-down approach based on reducing the size of the original particles by grinding, pickling, etc. [22–26]. Due to the high productivity and repeatability of processes, this approach is still widely used, although it has a significant drawback. The grinding of the material causes the surface structure of NPs to deteriorate due to the defects' formation.

The second approach, the so-called bottom-up approach, is an assembly of NPs from atoms or molecules [27–30]. Being more variable than the top-down method, it includes both chemical (chemical reduction, co-precipitation, seeding, microemulsion, sonoelectrodeposition, hydrothermal method, etc.) and physical (plasma method, microwave irradiation, pulser laser method, etc.) techniques.

An overview of top-down and bottom-up approaches is presented in Figure 2.

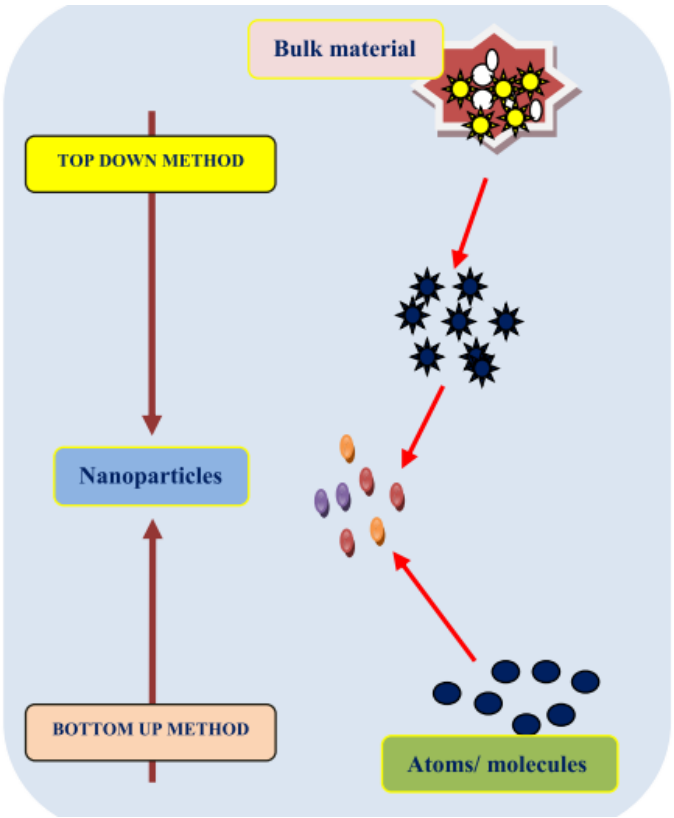

Figure 2. Top-down and bottom-up approaches to obtaining NPs. Reprinted with permission from ref. [31]. Copyright 2019 Elsevier.

Due to the very low solubility, precipitation from the solution is the most convenient bottom-up approach to obtain $BaSO_4$ NPs.

The bottom-up methods of producing $BaSO_4$ NPs involve the use of:

- Direct precipitation;
- Microemulsions;
- Microreactors;
- Membrane dispersion;
- Spinning disc reactors.

Despite the growing interest in $BaSO_4$ NPs, there are still no reviews on existing approaches to obtaining this product. To fill this gap, we have compiled data from the most relevant articles published over the past 25 years in this mini-review. This review focuses on recent advances in the production of $BaSO_4$ NPs using aforecited approaches, as well as their advantages and limitations. In addition, promising ways for furthering the development of methods for obtaining $BaSO_4$ nanoparticles are also discussed.

2. Top-Down Approach

In the top-down approach, starting bulk material is subjected to size reduction by different physical and chemical treatments, such as mechanical milling, laser ablation, and sputtering [32].

In the mechanical milling method, the bulk powder is placed into a container along with several heavy balls. Due to the high speed of the balls, the powder is given high mechanical energy, most likely by utilizing a planetary ball mill, attrition ball mill, or vibrating ball mill [33]. Under certain conditions, mechanical milling promotes repeated deformation, welding, and fracture of the mixture of reactants, which leads to different chemical modifications at the interface of NPs (mechanochemical synthesis) [34–39].

In the laser ablation method, the solid starting material is placed under a thin layer, then exposed to pulsed laser irradiation; the operation ensures reducing the particle size to nano level [31].

In the sputtering method, vaporization of a solid through sputtering with a beam of inert gas ions takes place [31].

Concerning $BaSO_4$ NPs, only two papers report obtaining this material by using a top-down approach; both were by the same authors exploiting mechanical milling in a stirred media mill [40,41]. The experimental set-up used is presented in Figure 3.

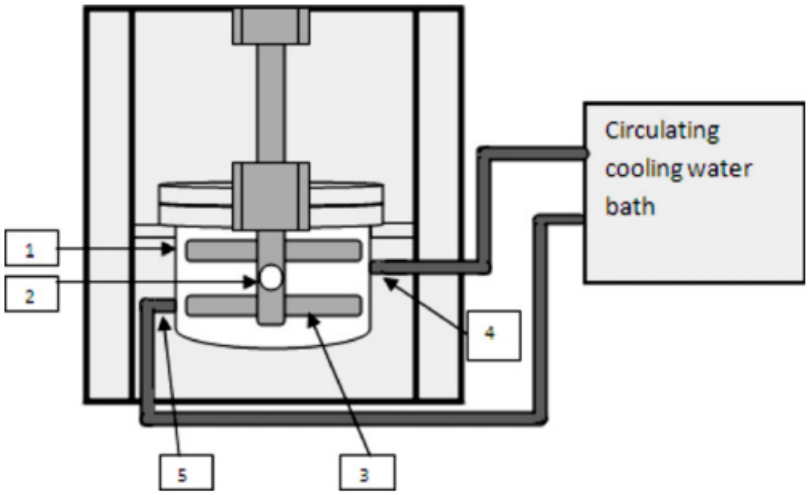

Figure 3. Experimental set-up for nanomilling. (1) Grinding chamber, (2) stirrer shaft, (3) stirrer pins, (4) cooling water in, (5) cooling water out. Reprinted with permission from ref. [40]. Copyright 2012 Elsevier.

By wet milling, the commercial barium sulfate in the presence of 2 wt% of the sodium salt of polyacrylic acid as a dispersant, NPs (~50 nm) were produced under optimal

conditions (pH of the suspension of 10.5; milling time of 180 min; solid mass fraction of 0.15; milling media loading of 60%; stirrer speed of 1200 rpm).

As a rule, top-down methods are easy to perform. Meanwhile, there are still no opportunities for preparing informal shaped and very small size particles. Another important issue limiting the use of these methods is a change in surface chemistry and physicochemical properties of nanoparticles [31].

3. Bottom-Up Strategy

3.1. Thermodynamic Origin

NPs arise and grow as a result of phase transformation processes. The emergence of a new phase is due to the desire of the system to move into a more stable state. Supersaturation of a solution with barium sulfate is the thermodynamic driving force of nucleation and growth of solid particles [42,43]. The formation of the target product is determined by the following ionic equation:

$$Ba^{2+} + SO_4^{2-} \rightarrow BaSO_4$$

Under equilibrium conditions, the chemical potentials of barium sulfate are equal in the liquid (1) and solid (2) phases [44]:

$$Ba^{2+} + SO_4^{2-} \rightarrow BaSO_4$$

where μ is the chemical potential of the component ($BaSO_4$, in this case) under the conditions of constant pressure (P), temperature (T), and concentration (C). Superscript "e" means the equilibrium state.

When supersaturated, there is a deviation from the equilibrium [44]:

$$\Delta\mu = \mu_2 - \mu_2^e > 0$$

This deviation is determined by the actual concentration of a solute (C) and the saturation concentration (C_s):

$$\Delta\mu = RTln\frac{C}{C_s}$$

where R is the universal gas constant.

In the case of a relatively high ionic strength of the solution, ion activities are used instead of concentrations, and the supersaturation of the solution (S_a) is defined as follows:

$$S_a = \sqrt{\frac{a_{Ba^{2+}} a_{SO_4^{2-}}}{K_{sp}}} = \gamma_{\pm} \sqrt{\frac{C_{Ba^{2+}} C_{SO_4^{2-}}}{K_{sp}}}$$

where $a_{Ba^{2+}}$ and $a_{SO_4^{2-}}$ are the activities of the corresponding ions, $C_{Ba^{2+}}$ and $C_{SO_4^{2-}}$ are the concentrations of the corresponding ions, $\gamma_{\pm}$ is the mean activity coefficient, and K_{sp} is the solubility product (for $BaSO_4$, $K_{sp} = 9.82 \times 10^{-11}$ mol^2/L^2 at 25 °C [45]).

Particle formation consists of two stages: the formation of nuclei and their growth. According to the classical theory of nucleation, the supersaturation of a system (ΔC) is determined by the difference between the concentration of a solute (C) and its concentration in a saturated solution (C_s):

$$\Delta C = C - C_s$$

For the formation of a nucleus, the appearance of a "solid–liquid" interface and a corresponding excess of free energy are necessary. The chemical potential of the particles in the solution (μ_C) may be written as:

$$\mu_C = \mu_C^0 + RTlnC$$

where μ_C^0 is the standard chemical potential of the component.

In a saturated solution, there is the following relationship between the chemical potential of the solid phase (μ_C) and the concentration of the saturated solution [44]:

$$\mu_s = \mu_C = \mu_C^0 + RTlnC_S$$

The growth of nuclei occurs by sequential attachment of particles from the solution to the solid surface. If the size of the nucleus is larger than the critical one, then such a process is thermodynamically favorable and practically irreversible.

The nucleation often plays the most important role in determining the resultant particle morphology and size distribution. Thus, the distribution of supersaturation in a reaction system is a key factor affecting the particles size distribution. The ideal process of obtaining NPs is that micromixing (mixing at the molecular level) of the reactants is achieved before a steady-state nucleation rate is established.

In many manufacturing technologies, the stabilization of obtained NPs in concentrated aqueous suspensions is required. Adsorption of a polymeric dispersant layer around the particle surface is mostly applied for this purpose. Polymer stabilization is based on the protection of the nanoparticle surface by a dense layer of organic molecules. The driving force behind this is the reduction in the number of possible configurations between two approaching particles; additionally, the osmotic pressure caused by the relatively high concentration of adsorbed polymer molecules between the two particles prevents the aggregation of these particles.

Suitable polymers for stabilization are those which, when dissolved, reduce the Gibbs' free energy. The interaction between polymer and solvent molecules is limited by conventional solvation processes, including dispersion interactions and the formation of hydrogen bonds. When approaching NPs completely covered with polymer molecules, the Gibbs' free energy rises, and the NPs repel.

3.2. Direct Precipitation

Direct precipitation (DP) is one of the most widely used methods for obtaining NPs because of the simplicity and availability of starting reagents. Due to the very poor solubility, the formed barium sulfate precipitates almost instantly with the formation of a white precipitate.

However, difficulties in controlling the size, and the strong tendency of particles to aggregate, significantly limit the use of this approach. This circumstance forces researchers to look for synthesis conditions that make it possible to obtain barium sulfate particles in a narrow size range and with a low tendency for aggregation.

The preparation conditions and particle size of $BaSO_4$ nanoparticles produced by direct precipitation and reported in the literature are provided in Table 1.

As a rule, this approach involves the preparation of aqueous solutions of barium compounds (mainly barium chloride) and ammonium sulfates or alkali metals (mainly sodium sulfate). In some cases, organic solvents such as ethanol [47,51] or benzene [52] were used, mixed with water. In about half of the described experiments, surfactants were used to stabilize the nanoparticles.

Bala et al. [47] prepared NPs of $BaSO_4$ in a liquid ethanol–water medium, by adding $(NH_4)_2SO_4$ aqueous solution to $BaCl_2$ dissolved in absolute ethanol. The precipitates were separated from the mother liquid and calcined for 1 h at 200 °C to obtain the final white powders. The average diameter of particles in an aqueous suspension was 24.3 nm while the full width at the half-maximum intensity of the distribution peak was 11.7 nm.

The particle size was significantly affected by the liquid (ethanol or water) used to wash the $BaSO_4$ precipitate: particles washed in ethanol were much smaller than those washed in water. It was suggested that this effect might be related to the adsorption of the ethanol onto the surface of the $BaSO_4$ particles, followed by encapsulation of the alcohol into the pores of the mentioned particles. The presence of ethoxy groups on the surface of the particles prevents their agglomeration, thereby providing high dispersion.

Table 1. Conditions for obtaining barium sulfate nanoparticles by direct precipitation, described in the literature.

Precursors	Medium	Stabilizer	Mean Particles Size, nm	Ref.
Na_2SO_4, $BaCl_2$	H_2O	gelatin	50.80 ± 0.02	[12]
Na_2SO_4, $BaCl_2$	H_2O	No	<100	[46]
$(NH_4)_2SO_4$, $BaCl_2$	$H_2O - C_2H_5OH$	No	24.3	[47]
H_2SO_4, $BaCl_2$, $Ba(OH)_2$	H_2O	No	4–92	[48]
$K_2S_2O_8$, $BaCl_2$	H_2O	(2-(methacryloyloxy)ethyldimethyl-(3-sulfopropyl)ammoniumhydroxide; 3-sulfopropylmethacrylate potassium salt; 2-acrylamido-2- methylpropane sulfonic acid.	10–20	[49]
$(NH_4)_2SO_4$, H_2SO_4, $BaCl_2$	H_2O	octadecyl dihydrogen phosphate	76	[50]
Na_2SO_4, $Ba(NO_3)_2$	H_2O	sodium hexametaphosphate	30–55	[51]
Na_2SO_4, $BaCl_2$	H_2O	dodecyl trimethyl ammonium bromide	180–190	[52]
$(NH_4)_2SO_4$, $BaCl_2$	$H_2O - C_2H_5OH$	dodecyl benzene sulfonic acid	46	[53]
Na_2SO_4, $BaCl_2$	H_2O	No	30.4	[54]
Na_2SO_4, $BaCl_2$	$H_2O - C_6H_6$	No	35.9	[54]
Na_2SO_4, $BaCl_2$	H_2O	carboxymethylcellulose	45 ± 12	[55]
Na_2SO_4, $BaCl_2$	H_2O	sodium dodecyl sulfate	80–150	[56]
* $(NH_4)_2SO_4$, $BaCl_2$	H_2O	sodium lauryl sulfate	9	[57]
* Na_2SO_4, $BaCl_2$	H_2O	cetyltrimethylammonium bromide	55.6	[58]

* Ultrasound has been applied.

Highly crystalline $BaSO_4$ NPs obtaining procedure has been described by Sifontes and co-workers [48]; $Ba(OH)_2 \cdot 8H_2O$, $BaCl_2 \cdot 2H_2O$, as well as aqueous sulfuric acid were the precursors. The obtained precipitate was washed and filtered with distilled water several times and was frozen at −26 °C for 1 day. The nanoparticles size was between 2.6 and 20 nm, with an average value of 14.5 nm. The proposed method's main premise was quenching, which involves cooling rapidly to a lower temperature. The growth of $BaSO_4$ particles is stopped by quenching with cold water, which eliminated the need for additives as stabilizers.

An unusual strategy to control the nucleation and growth of $BaSO_4$ nanoparticles was proposed in [49]. Unlike other techniques, sulfate ions are in situ generated here by decomposition of potassium persulfate in an alkaline medium:

$$S_2O_8^{2-} + 2OH^- \leftrightarrow 2SO_4^{2-} + 2OH\bullet$$

A new difunctional surface modification agent, -(2-(methacryloyloxy)ethyldimethyl–(3-sulfopropyl)ammoniumhydroxide, was applied as surfactant. This approach allowed manipulating the nucleation and growth of the $BaSO_4$ particles and significantly reducing the particle size, up to several nanometers.

In some cases, the surface modification of barium sulfate NPs was carried out to give them specific properties.

Octadecyl dihydrogen phosphate (n-$C_{18}H_{37}OPO_3H_2$, ODP) was applied as a modifying agent in the one-step process of $BaSO_4$ precipitation [50]. ODP served two purposes in this case. A thin layer of barium alkyl phosphates, which was formed and coated onto the surface of NPs, makes them hydrophobic:

$$Ba^{2+} + 2n - C_{18}H_{37}OPO_3H_2 \longleftrightarrow Ba - (n - C_{18}H_{37}OPO_3H)_2 + 2H^+$$

$$Ba^{2+} + n - C_{18}H_{37}OPO_3H_2 \longleftrightarrow Ba - (n - C_{18}H_{18}H_{37}OPO_3) + 2H^+$$

Furthermore, ODP controls the particle size and morphology of $BaSO_4$ NPs formed by the reaction between $BaCl_2$ and $(NH_4)_2SO_4$.

NPs of $BaSO_4$, functionalized by a difunctional surface modification agent, (2-(methacryloyloxy)ethyldimethyl-(3-sulfopropyl)ammoniumhydroxide (MSAH), were examined as a filler in bone cements [49]. It was revealed that functionalized NPs effectively improved the bending modulus and compressive strength of the poly (methyl methacrylate) bone cement; moreover, the bone cement with MSAH-functionalized NPs of $BaSO_4$ exhibited good radiopacity. Improved biocompatibility of functionalized NPs compared to the bare $BaSO_4$ particles was also demonstrated.

Sooch and co-workers developed a technique of obtaining NPs of $BaSO_4$ capped with gelatin and doped with four different metals [12]. The obtained functionalized NPs were shown to have enhanced antimicrobial potential and cytotoxicity.

NPs with a size of around 10 nm or smaller have been synthesized in just a small portion of the works devoted to the direct $BaSO_4$ precipitation; the vast majority of the proposed methods provided an average size in the range of about 25–150 nm.

3.3. Microemulsion Method

The microemulsion is a popular method of obtaining NPs, where microemulsions are an isotropic and thermodynamically stable mixture of oil, water, and surfactant, or in combination with a cosurfactant [59–63]. Microemulsions can be either direct (oil dispersed in water) or reversed (water dispersed in oil). In the simplest case of two water-soluble but oil-insoluble reagents, one of the reagents dissolves in water micro drops of a w/o microemulsion, and the other dissolves in water micro drops of another w/o microemulsion. The two microemulsions are then mixed. Due to the small size of the droplets, they take part in Brownian motion. They continuously collide, forming dimers and other aggregates. Such aggregates have a short lifetime and quickly disintegrate into drops of the original size. As a result of continuous processes of coalescence and spontaneous dispersion, the content of water microdroplets of both microemulsions is evenly distributed over all drops in which the reaction takes place. The reaction product eventually precipitates out.

In almost all cases, microemulsions contain an appropriate amount of surfactant. The surfactant molecules that are located in the w/o interface significantly reduce the interfacial tension of the interface, thereby ensuring the stability of the emulsion.

This method allows the production of compounds of a significant purity degree and high dispersion with a controlled particle size distribution, as well as polycomponent particles with a uniform distribution of components. One of the main advantages of this method is the ability to control the size and shape of the resulting NPs.

The schematic diagrams of particle formation and particle coagulation in a microemulsion system are presented in Figures 4 and 5, respectively.

In the preparation of barium sulfate NPs, the corresponding precursors are initially contained in various microemulsions, which, when mixed, form the desired product. Liquid hydrocarbons and polyoxyethylene derivatives are mainly used as organic components of microemulsions; the precursors are the same compounds as in the cases of direct precipitation (Table 2).

Qi et al. [66] synthesized spherical and cubic $BaSO_4$ NPs by using Triton X-100/n-hexanol/cyclohexane/water w/o microemulsions. As the water content in microemulsions increased, the particle shape changed from spherical to cubic. Triton X-100 is a non-ionic surfactant that has also been applied for $BaSO_4$ NPs obtained by Ivanova et al. [4] and Meagher et al. [21]. In both studies, monodisperse $BaSO_4$ NPs (~10 nm in diameter) were synthesized using w/o nanoemulsions. In [21], as-prepared NPs were subsequently encapsulated by dextran. This operation increased the NPs diameter to ~40 nm but enabled them to be readily redispersed in water. Moreover, encapsulated NPs were stable in the colloidal form for more than 1 month.

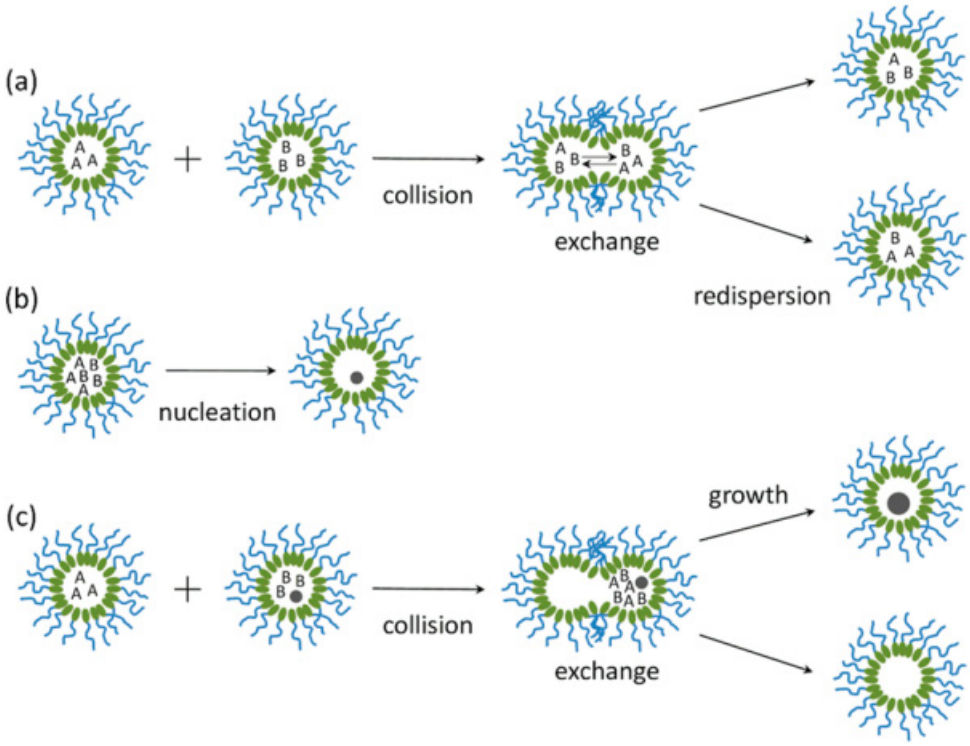

Figure 4. Schematic representation of particle formation in a microemulsion system: (**a**) fusion-fission and mass transfer between microemulsion droplets; (**b**) nucleation in a supersaturated droplet; (**c**) growth of a particle through the exchange of reactants during a collision. Reprinted with permission from ref. [64]. Copyright 2014 American Chemical Society.

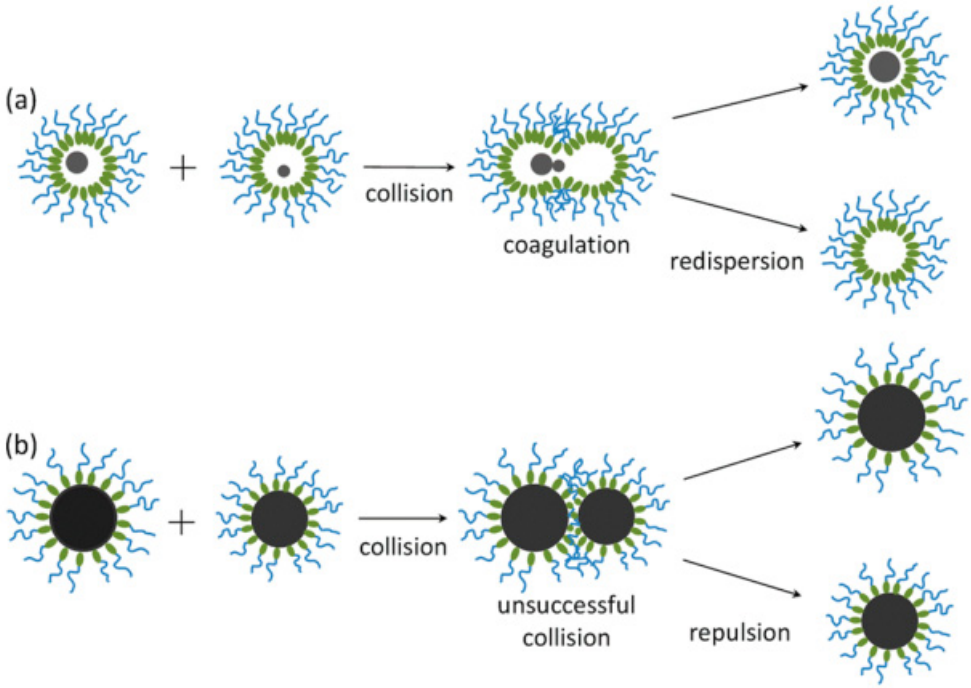

Figure 5. Schematic diagram of particle coagulation in a microemulsion system: (**a**) coagulation of microscopic particles trapped in microemulsion droplets; (**b**) failure of two big colloidal particles to collide. Reprinted with permission from ref. [64]. Copyright 2014 American Chemical Society.

Table 2. Conditions for obtaining barium sulfate nanoparticles by using microemulsions, described in the literature.

Precursors	Organic Parts of Microemulsion	Mean Particles Size, nm	Ref.
$(NH_4)_2SO_4$, $BaCl_2$	cyclohexane; benzene; Triton X-100; t-Oct-C6H4-(OCH_2CH_2)xOH (x = 9–10); 1-hexanol.	13	[21]
$K_2S_2O_8$, H_2SO_4, $BaCl_2$	poly(oxyethylene)$_5$ phenol ether; poly(oxyethylene)$_9$ phenol ether.	10–20	[65]
$(NH_4)_2SO_4$, $Ba(OAc)_2$	Triton X-100; n-hexanol; cyclohexane.	10	[66]

Na_2SO_4, $BaCl_2$	sodium bis(2-ethylhexylsulfosuccinate;
	poly(oxyethylene-4-dodecyl ether);
	didodecyldimethylammonium bromide;
	decane;
	dodecane;
	isooctane.
		2–4	[67]

$(NH_4)_2SO_4$, H_2SO_4, $BaCl_2$	poly(ethylene glycol) octylphenyl ether; Triton X-100; n-hexyl alcohol; cyclohexane.	5–10	[68]
K_2SO_4, $BaCl_2$	Marlipal O13/40; cyclohexane.	6 ± 2	[69]

Commercial ethoxylated iso-tridecanol, widely known as non-ionic technical surfactant Marlipal O13/40, was used to obtain $BaSO_4$ NPs by using a semi-batch reactor [69]. Almost monodisperse NPs (3–8 nm in diameter) were precipitated in a microemulsion droplet population.

Empirical optimization of the conditions for obtaining NPs by the microemulsion method is associated with significant time and other costs due to the huge variability of possible processes. Population balance modeling (PBM) is widely used to solve this problem [70–74]. PBM describes the evolution of a population of particles in the processes of crystallization, precipitation, polymerization, etc. [75–77].

Two different modes for the initialization of the precipitation reaction are generally accepted. According to the first mode, one reactant moves by mass transport from the continuous phase into the microemulsion droplets which already contain the other reactant [78,79]. The second model assumes that both reactants dissolve in two separate microemulsions, which are then combined by pouring one of the two microemulsions into a stirred tank reactor that is partly filled with the other microemulsion [80]. A scheme of this process is presented in Figure 6 along with a TEM picture of $BaSO_4$ NPs.

A simplified, zero-dimensional (homogeneous) PBM describing the precipitation of $BaSO_4$ NPs in a microemulsion droplet population has been performed by Oncul et al. [81]. The model, obtained by computational fluid dynamic simulations, was implemented for the three-dimensional real case analysis of the reaction process in a semi-batch reactor. The obtained results of computations have demonstrated good agreement with the experimental data for stoichiometric cases.

Based on the experimental results described in ref. [82], Niemann and Sundmacher proposed a discrete PBM with the introduction of physically motivated assumptions at $BaSO_4$ precipitation in w/o emulsion [78]. According to the model, nuclei are found to be formed heterogeneously. The model requires low computational effort and produces a solution of high accuracy.

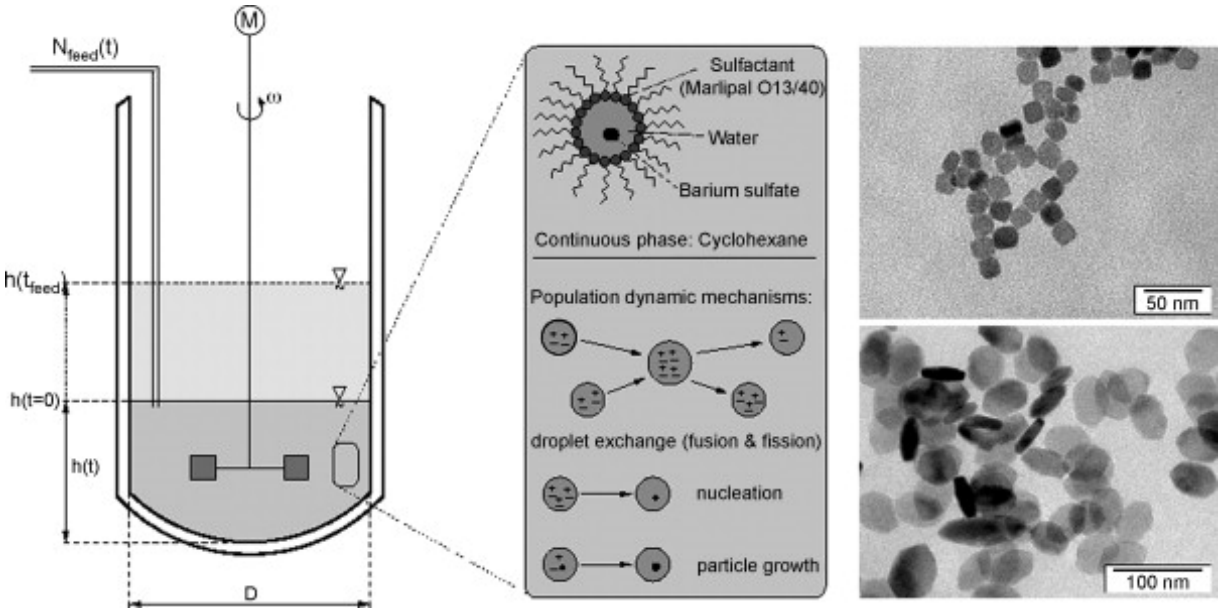

Figure 6. Process diagram, population dynamics, and TEM image of generated $BaSO_4$ NPs. Reprinted with permission from ref. [78]. Copyright 2008 Elsevier.

By using a PBM, it was shown that at low initial reactants concentration, coagulation can have a significant effect on $BaSO_4$ NPs precipitation in nonionic inverse microemulsion systems [64]. The coagulation effect is found to be responsible for the bimodal particle size distribution described in the literature. Furthermore, the effect of electrolyte concentration on the surfactant headgroup area was investigated. The obtained kinetic parameters demonstrate that nucleation, growth, and coagulation rate constants increase with decreasing electrolyte concentration.

In general, the use of microemulsions made it possible to obtain nanoparticles with a size of 3–10 nm, which is much smaller than those synthesized by direct precipitation. Nevertheless, a large amount of surfactant is required. Moreover, long processing time and the use of organic solutions that can be toxic may also limit the use of this approach.

3.4. Obtaining $BaSO_4$ NPs in Microreactors

A prospective approach to obtaining NPs is using microfluidic reactors or microreactors. Compared to batch-wise synthesis approaches, microfluidic technologies provide better control of the amount of reagents and allow mixing them uniformly on the microscale [83–87]. This approach shows promise for commercial-scale synthesis of NPs; the small yield of the product from microreactors can be addressed by parallel processing. Depending on their flow type, microreactors can be classified as continuous flow (reaction and precipitation occur in a single fluid phase inside the microchannel) and droplet-based or segmented flow (reaction occurs within discrete droplets that pass through the microreactor surrounded by an immiscible carrier phase).

Generally, T-or Y-shaped micromixers are used as the mixing units for obtaining $BaSO_4$ NPs [88]. Table 3 summarizes some information about the main constructional and operating parameters when producing $BaSO_4$ NPs in T- and Y-microreactors that has been gathered from the literature.

Table 3. Obtaining conditions on the particle size of $BaSO_4$ NPs produced in T- and Y-microreactors described in the literature.

Type of Microreactor	Reaction System	Channel Size, μm	Ba^{2+}/SO_4^{2-} Molar Ratio	Ba^{2+} Solution Concentration, mol/L	Flow Rate, mL/min	Mean Particle Size, nm	Ref.
T	Microemulsion	500	1	0.1	0.8	15	[89]
T	Liquid-liquid	1000	3	0.7	180	35	[90]
T	Liquid-liquid	600 × 300	1.5	0.5	24	91	[91]
T	Two-phase	830 × 1000	5	0.5	6.5	300	[92]
Y	-	500	1	0.1	30	200	[93]
Y	-	500	5	≤0.5	600	40	[94]

Wang et al. [95] developed a microporous tube-in-tube microchannel reactor exhibiting the combined effects of many T-type microchannels. The total flow rate of up to 9 L/min ensured increased production capacities of the microreactor and $BaSO_4$ NPs with an average size of 37 nm were obtained. Nevertheless, concentrations of reagents in solutions were still relatively low (0.35 mol/L for both reactants).

Sen et al. described a droplet-based microfluidic system comprising a simple microfluidic junction and a PTFE microbore tube to continuously obtain $BaSO_4$ NPs with a mean particle size of 65 nm [96].

$BaCl_2$ and Na_2SO_4 concentrations close to their saturated concentrations were successfully used to obtain $BaSO_4$ NPs by Wu et al. [88]. A commercially available micromixer, SIMM-V2, with a mixing element of 2 × 16 interdigital microchannels with a size of 45 μm (width) × 200 μm (depth) for each of the 32 channels, was applied for this purpose. Interdigital feeds, providing multiple outlet ports with alternately arranged fluids, operate on a more complex mixing principle than the T- or Y- micromixers. By using Ba^{2+}/SO_4^{2-} at a molar ratio of 1.2 and a total flow rate of 50 mL/min, the NPs with a mean particle size of 28 nm were obtained at a production capacity of 2 kg/h.

The effect of ultrasound on mixing and the precipitation of $BaSO_4$ NPs in microreactors have been studied by Pohl and co-workers [97]. Initially, a conical chamber (10 mL) was applied to study the effect of micromixing quality and the cavitation intensity on the precipitation process. Then, a cavitational chamber (2.5 mL) was used as an optimized conical reactor. It was demonstrated that in both reactors, low ultrasonic output between 20 and 40 W improves the precipitation results. NPs with a particle size of 200 nm can be produced at a low feed rate of 0.8 L/h under ultrasonic irradiation, whereas much higher feed rates of 6 L/h are needed to achieve the same results without ultrasound.

The higher surface-to-volume ratio, which can reach 100,000 m^2/m^3, taken together with the opportunity to control the size and shape of produced NPs, provides the microreactor approach with significant competitive advantages [98]. The method's drawbacks include the high cost of microreactors and the risk of NPs blocking micropores during their rapid development. Besides, precursor solutions must wet the hydrophilic surface of pore walls, which imposes additional requirements on the composition of solutions. By and large, these limitations of this approach have not yet been overcome.

3.5. Membrane Dispersion

It was mentioned above that the distribution of supersaturation in a reaction system has a decisive influence on particle morphology and size distribution, and mixing at almost the molecular level (micromixing) is the ideal process for obtaining NPs. Membrane dispersion (in some cases referred to as membrane separation) is an effective approach that provides acceptable dosing of one of the components entering the reaction mixture when obtaining NPs [99–103].

The process of obtaining nanoparticles is implemented in a membrane reactor, which operates on the following principle (Figure 7a,b) [104]. A solution of one of the components (for example, Na_2SO_4) contained in the inner part of the reactor penetrates through the micropores of the membrane into the outer part containing a solution of another component

(for example, $BaCl_2$). The driving force of the process is the higher pressure in the inner part compared to that in the outer part of the reactor ($P_{in} > P_{out}$). It is also possible to carry out the process at $P_{in} < P_{out}$ when the components of the solution in the outer particles of the reactor penetrate the inner one.

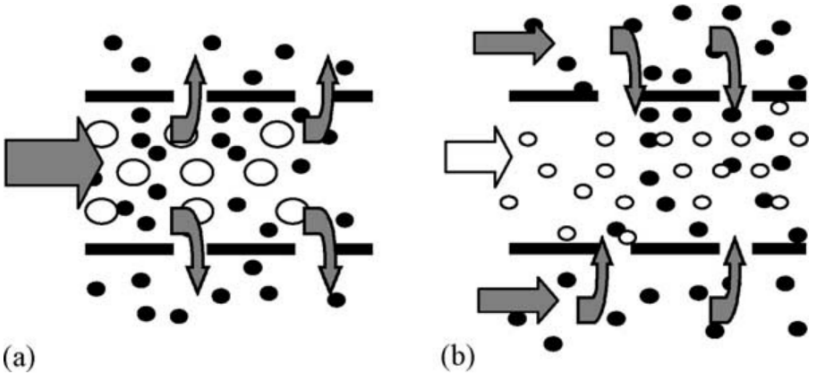

Figure 7. Principles of obtaining NPs through membrane dispersion (the balls represent the molecules): (**a**) $P_{in} > P_{out}$, (**b**) $P_{in} < P_{out}$. Reprinted with permission from ref. [104]. Copyright 2002 Elsevier.

Zhiqian and Zhongzhou obtained $BaSO_4$ NPs by using a membrane reactor, in which the Na_2SO_4 solution permeated through the micropores of the ultrafiltration membrane gradually into $BaCl_2$ solution [104]. Under the optimized conditions (SO_4^{2-}/Ba^{2+}molar ratio of 2; membrane molecular weight cut-off of 1000; transmembrane pressures of 0.010 MPa; linear flow rate of 0.589 m/s; the absolute temperature of 288 K; concentration of $BaCl_2$ of 0.005 mol/L; the initial volume of $BaCl_2$ solutions of 80 mL), the size of obtained $BaSO_4$ NPs was ~60 nm.

Chen and co-workers have developed new membrane dispersion technology for producing $BaSO_4$ NPs [105]. The process integrates direct chemical precipitation and membrane emulsification. A 20% ethyl alcohol in water solution is used as the solvent instead of pure water, which ensured the particles size decreases from 70 to 20 nm.

Introducing microbubbles into the working system with the membrane dispersion microreactor has been successfully applied for $BaSO_4$ NPs synthesis [15]. Microbubbles ensured efficient mixing of the reactant at high concentrations (up to 0.32 mol/L Na_2SO_4 and 2.2 mol/L $BaSO_4$), which made it possible to obtain NPs with an average size of 40 nm.

Along with the advantages, membrane technologies for obtaining nanoparticles also have drawbacks [106]. The main factor limiting the use of this approach is the high cost of membranes. Furthermore, irreversible processes of membrane fouling and damage are likely during the operation of the membrane reactor. Meanwhile, fouling of membranes can be minimized through the selection of suitable membrane materials, rinsing the membrane regularly, and optimizing operating conditions

3.6. Obtaining $BaSO_4$ NPs in Spinning Disc Reactors

The *spinning disk reactor* (SDR) is the apparatus with the best mass and heat transfer characteristics of all chemical reactor types [107].

In an SDR, a fast-moving liquid microfilm is formed on a rotating disk by centrifugal force [108]. Due to the high centrifugal and shear forces exerted on the developed thin liquid film with high micromixing efficiency, SDR has a high transfer rate and a short mixing time, which ensure high performance in the synthesis of nanoparticles. NPs of Ag [109], ZnO [110], CuO [111], and TiO_2 [112] were synthesized through the SDR technique.

The efficiency of using SDR to produce $BaSO_4$ NPs has improved significantly in recent years. In 2002, Cafiero and co-workers obtained NPs with a mean particle size of 700 nm [113]. In 2009, Dehkordi and Vafaeimanesh obtained $BaSO_4$ NPs with a size of ~38 nm in diameter from supersaturated aqueous solutions of $BaCl_2$ and Na_2SO_4 [114].

The mean particle size of 27 nm was achieved by Jacobsen and Hinrichsen in 2012 [115]. The new configuration of SDR for obtaining NPs was described by Farahani and co-workers in 2017 [116]. The reactor's unique design, which consists of two coaxial rotating disks positioned horizontally in a cylindrical chamber, made it possible to improve micromixing efficiency. This double SDR (DSDR) demonstrated higher efficiency compared to conventional SDRs. Specifically, smaller particles (mean size of 23.4 nm) were obtained. Furthermore, a narrower particles size distribution was achieved.

A significant reduction in the average particle size of barium sulfate has been achieved using a new high-speed spinning disk reactor (HSSDR) [117]. Exploiting the high rotational disk speed (from 5000 to 15,000 rpm) yielded particles with an average size of 16.4 nm. Moreover, it was stated that the cost of running HSSDR is lower than that of DSDR proposed in ref. [116].

The use of SDR for the synthesis of nanomaterials, for instance, $BaSO_4$ NPs, is an attempt to overcome the problems associated with scaling-up production and achieve greater control of the size of the NPs produced. However, the use of SDR comes with a number of difficulties. This system requires more sophisticated equipment than conventional ones, resulting in higher equipment costs [118]. The energy needed for disc rotation and to overcome pressure drop also influences the operation costs of SDR due to the high dissipation rate of the applied energy. Besides, the extremely high disk rotation speed (up to 15,000 rpm) significantly increases the risk of mechanical failure and places high demands on SDR materials and disk balancing in the reactor.

4. Conclusions and Future Perspectives

$BaSO_4$ NPs are becoming more widely used in various fields. Accordingly, the demand for this material is increasing. Two fundamentally different approaches are used to obtain these NPs. According to the first one (top-down approach), the bulk material is milled to obtain nanosized particles. However, this approach does not allow one to control the size and shape of the particles, and it also leads to a change in the physicochemical properties of the milled material. More promising is the other (bottom-up) approach, according to which the target product is assembled from the smallest particles, atoms or molecules. Due to the very low solubility of barium sulfate, its liquid-phase synthesis with subsequent precipitation is very convenient. The biggest problem in implementing this approach is the control of reagents mixing: direct precipitation leads to the uncontrolled growth of $BaSO_4$ crystals. This issue can be partly solved by using microemulsions, microreactors, membrane dispersion, and spinning disc reactors. However, unresolved issues remain, e.g., many of the solvents used are toxic, the resulting solid particles of barium sulfate clog the channels of the microreactors, and there are irreversible fouling and destruction of membranes. In addition, many developed methods for obtaining these nanoparticles are difficult to scale.

In our opinion, further development of methods for obtaining $BaSO_4$ NPs will proceed as follows. Liquid phase synthesis will be predominant in the preparation of this product. Due to the simplicity and availability of starting reagents, precipitation from aqueous solutions will remain the most common method. The high precipitation rate from aqueous solutions, however, limits the ability to control particle size and morphology. To solve this problem, an approach seems practicable, assuming there is a relatively slow reaction of sulfate ion formation in the solution (for example, through the use of $S_2O_8^{2-}$ anions [46]). The use of toxic organic reagents, mainly in the microemulsion method, should be fully justified. To intensify the processes of mass and heat transfer, particularly micromixing, the design of reactors should be optimized. Population balance modeling is an effective tool for this purpose; by exploiting hydrodynamics in a controlled manner, this approach allows for the improvement of process quality to obtain $BaSO_4$ NPs in a narrow size distribution range. Addressing these issues, either completely or locally, will significantly expand the scope of the industrial application of $BaSO_4$ NPs.

Author Contributions: Methodology, T.K., A.B. and D.G.; writing—original draft preparation, R.N. and K.K.; writing—review and editing, R.N., D.G. and T.K. All authors have read and agreed to the published version of the manuscript.

Funding: This research was funded by the Science Committee of the Ministry of Education and Science of the Republic of Kazakhstan (Grant No. OR11465430).

Institutional Review Board Statement: Not applicable.

Informed Consent Statement: Not applicable.

Data Availability Statement: The data supporting the results can be made available from the corresponding author upon request.

Conflicts of Interest: The authors declare no conflict of interest.

References

1. Baig, N.; Kammakakam, I.; Falath, W. Nanomaterials: A review of synthesis methods, properties, recent progress, and challenges. *Mater. Adv.* **2021**, *2*, 1821–1871. [CrossRef]
2. Srinoi, P.; Chen, Y.T.; Vittur, V.; Marquez, M.D.; Lee, T.R. Bimetallic nanoparticles: Enhanced magnetic and optical properties for emerging biological applications. *Appl. Sci.* **2018**, *8*, 1106. [CrossRef]
3. Elahi, N.; Kamali, M.; Baghersad, M.H. Recent biomedical applications of gold nanoparticles: A review. *Talanta* **2018**, *184*, 537–556. [CrossRef] [PubMed]
4. Urakaev, F.K.; Khan, N.V.; Shalabaev, Z.S.; Tatykaev, B.B.; Nadirov, R.K.; Burkitbaev, M.M. Synthesis and photocatalytic properties of silver chloride/silver composite colloidal particles. *Colloid J.* **2020**, *82*, 76–80. [CrossRef]
5. Sadeghi-Aghbash, M.; Rahimnejad, M. Zinc Phosphate Nanoparticles: A Review on Physical, Chemical, and Biological Synthesis and their Applications. *Curr. Pharm. Biotechnol.* **2022**, *23*. [CrossRef] [PubMed]
6. Waghmode, M.S.; Gunjal, A.B.; Mulla, J.A.; Patil, N.N.; Nawani, N.N. Studies on the titanium dioxide nanoparticles: Biosynthesis, applications and remediation. *SN Appl. Sci.* **2019**, *1*, 310. [CrossRef]
7. Tighe-Neira, R.; Carmora, E.; Recio, G.; Nunes-Nesi, A.; Reyes-Diaz, M.; Alberdi, M.; Rengel, Z.; Inostroza-Blancheteau, C. Metallic nanoparticles influence the structure and function of the photosynthetic apparatus in plants. *Plant Physiol. Biochem.* **2018**, *130*, 408–417. [CrossRef]
8. Kannan, K.; Radhika, D.; Sadasivuni, K.K.; Reddy, K.R.; Raghu, A.V. Nanostructured metal oxides and its hybrids for photocatalytic and biomedical applications. *Adv. Colloid Interface Sci.* **2020**, *281*, 102178. [CrossRef]
9. Roy, S.D.; Das, K.C.; Dhar, S.S. Conventional to green synthesis of magnetic iron oxide nanoparticles; its application as catalyst, photocatalyst and toxicity: A short review. *Inorg. Chem. Commun.* **2021**, *134*, 109050. [CrossRef]
10. Yang, B.; Peng, S.; Choy, W.C. Inorganic top electron transport layer for high performance inverted perovskite solar cells. *EcoMat* **2021**, *3*, e12127. [CrossRef]
11. Zhuang, Q.; Wang, H.; Zhang, C.; Gong, C.; Li, H.; Chen, J.; Zang, Z. Ion diffusion-induced double layer doping toward stable and efficient perovskite solar cells. *Nano Res.* **2022**, 1–9. [CrossRef]
12. Sooch, B.S.; Mann, M.K.; Sharma, M. Metal-doped barium sulphate nanoparticles decorated with gelatin as antibacterial agents. *J. Clust. Sci.* **2021**, *32*, 1141–1154. [CrossRef]
13. Reissig, F.; Zarschler, K.; Hübner, R.; Pietzsch, H.J.; Kopka, K.; Mamat, C. Sub-10 nm Radiolabeled Barium Sulfate Nanoparticles as Carriers for Theranostic Applications and Targeted Alpha Therapy. *Chemistryopen.* **2020**, *9*, 797–805. [CrossRef] [PubMed]
14. Akyol, E.; Cedimagar, M.A. Size and morphology controlled synthesis of barium sulfate. *Cryst. Res. Technol.* **2016**, *51*, 393–399. [CrossRef]
15. Du, L.; Wang, Y.J.; Lu, Y.C.; Luo, G.S. Process intensification of $BaSO_4$ nanoparticle preparation with agitation of microbubbles. *Powder Technol.* **2013**, *247*, 60–68. [CrossRef]
16. Konduru, N.; Keller, J.; Ma-Hock, L.; Gröters, S.; Landsiedel, R.; Donaghey, T.C.; Molina, R.M. Biokinetics and effects of barium sulfate nanoparticles. *Part. Fibre Toxicol.* **2014**, *11*, 55. [CrossRef]
17. Schwotzer, D.; Ernst, H.; Schaudien, D.; Kock, H.; Pohlmann, G.; Dasenbrock, C.; Creutzenberg, O. Effects from a 90-day inhalation toxicity study with cerium oxide and barium sulfate nanoparticles in rats. *Part. Fibre Toxicol.* **2017**, *14*, 23. [CrossRef]
18. Mohn, D.; Zehnder, M.; Imfeld, T.; Stark, W.J. Radio-opaque nanosized bioactive glass for potential root canal application: Evaluation of radiopacity, bioactivity and alkaline capacity. *Int. Endod. J.* **2010**, *43*, 210–217. [CrossRef]
19. Molina, R.M.; Konduru, N.V.; Queiroz, P.M.; Figueroa, B.; Fu, D.; Ma-Hock, L.; Groeters, S.; Schaudien, D.; Brain, J.D. Fate of barium sulfate nanoparticles deposited in the lungs of rats. *Sci. Rep.* **2019**, *9*, 8163. [CrossRef]
20. Aninwene, G.E.; Stout, D., II; Yang, Z.; Webster, T.J. Nano-$BaSO_4$: A novel antimicrobial additive to pellethane. *Int. J. Nanomed.* **2013**, *8*, 1197.
21. Meagher, M.J.; Leone, B.; Turnbull, T.L.; Ross, R.D.; Zhang, Z.; Roeder, R.K. Dextran-encapsulated barium sulfate nanoparticles prepared for aqueous dispersion as an X-ray contrast agent. *J. Nanoparticle Res.* **2013**, *15*, 2146. [CrossRef]

22. Amendola, V.; Meneghetti, M.; Granozzi, G.; Agnoli, S.; Polizzi, S.; Riello, P.; Sangregorio, C. Top-down synthesis of multifunctional iron oxide nanoparticles for macrophage labelling and manipulation. *J. Mater. Chem.* **2011**, *21*, 3803–3813. [CrossRef]
23. Wijesena, R.N.; Tissera, N.; Kannangara, Y.Y.; Lin, Y.; Amaratunga, G.A.; de Silva, K.N. A method for top down preparation of chitosan nanoparticles and nanofibers. *Carbohydr. Polym.* **2015**, *117*, 731–738. [CrossRef] [PubMed]
24. Yang, J.; Ling, T.; Wu, W.T.; Liu, H.; Gao, M.R.; Ling, C.; Du, X.W. A top–down strategy towards monodisperse colloidal lead sulphide quantum dots. *Nat. Commun.* **2013**, *4*, 1695. [CrossRef] [PubMed]
25. Reverberi, A.P.; Kuznetsov, N.T.; Meshalkin, V.P.; Salerno, M.; Fabiano, B. Systematical analysis of chemical methods in metal nanoparticles synthesis. *Theor. Found. Chem. Eng.* **2016**, *50*, 59–66. [CrossRef]
26. Van Eerdenbrugh, B.; Van den Mooter, G.; Augustijns, P. Top-down production of drug nanocrystals: Nanosuspension stabilization, miniaturization and transformation into solid products. *Int. J. Pharm.* **2008**, *364*, 64–75. [CrossRef]
27. Chan, H.K.; Kwok, P.C.L. Production methods for nanodrug particles using the bottom-up approach. *Adv. Drug Deliv. Rev.* **2011**, *63*, 406–416. [CrossRef]
28. Ortega, S.; Ibáñez, M.; Liu, Y.; Zhang, Y.; Kovalenko, M.V.; Cadavid, D.; Cabot, A. Bottom-up engineering of thermoelectric nanomaterials and devices from solution-processed nanoparticle building blocks. *Chem. Soc. Rev.* **2017**, *46*, 3510–3528. [CrossRef]
29. Pini, M.; Rosa, R.; Neri, P.; Bondioli, F.; Ferrari, A.M. Environmental assessment of a bottom-up hydrolytic synthesis of TiO_2 nanoparticles. *Green Chem.* **2015**, *17*, 518–531. [CrossRef]
30. Sierra-Pallares, J.; Huddle, T.; García-Serna, J.; Alonso, E.; Mato, F.; Shvets, I.; Lester, E. Understanding bottom-up continuous hydrothermal synthesis of nanoparticles using empirical measurement and computational simulation. *Nano Res.* **2016**, *9*, 3377–3387. [CrossRef]
31. Jamkhande, P.G.; Ghule, N.W.; Bamer, A.H.; Kalaskar, M.G. Metal nanoparticles synthesis: An overview on methods of preparation, advantages and disadvantages, and applications. *J. Drug Deliv. Sci. Technol.* **2019**, *53*, 101174. [CrossRef]
32. Meyers, M.A.; Mishra, A.; Benson, D.J. Mechanical properties of nanocrystalline materials. *Prog. Mater. Sci.* **2006**, *51*, 427–556. [CrossRef]
33. Rajput, N. Methods of preparation of nanoparticles-a review. *Int. J. Adv. Eng. Technol.* **2015**, *7*, 1806.
34. Tsuzuki, T.; McCormick, P.G. Mechanochemical synthesis of nanoparticles. *J. Mater. Sci.* **2004**, *39*, 5143–5146. [CrossRef]
35. Baláž, M.; Daneu, N.; Balážová, Ľ.; Dutková, E.; Tkáčiková, Ľ.; Briančin, J.; Baláž, P. Bio-mechanochemical synthesis of silver nanoparticles with antibacterial activity. *Adv. Powder Technol.* **2017**, *28*, 3307–3312. [CrossRef]
36. Shalabayev, Z.; Baláz, M.; Daneu, N.; Dutková, E.; Bujnáková, Z.; Kanuchová, M.; Burkitbayev, M. Sulfur-mediated mechanochemical synthesis of spherical and needle-like copper sulfide nanocrystals with antibacterial activity. *ACS Sustain. Chem. Eng.* **2019**, *7*, 12897–12909. [CrossRef]
37. Baláž, M.; Zorkovská, A.; Urakaev, F.; Baláž, P.; Briančin, J.; Bujňáková, Z.; Gock, E. Ultrafast mechanochemical synthesis of copper sulfides. *RSC Adv.* **2016**, *6*, 87836–87842. [CrossRef]
38. Baláž, M.; Dobrozhan, O.; Tešinský, M.; Zhang, R.Z.; Džunda, R.; Dutková, E.; Baláž, P. Scalable and environmentally friendly mechanochemical synthesis of nanocrystalline rhodostannite ($Cu_2FeSn_3S_8$). *Powder Technol.* **2021**, *388*, 192–200. [CrossRef]
39. Dutková, E.; Čaplovičová, M.; Škorvánek, I.; Baláž, M.; Zorkovská, A.; Baláž, P.; Čaplovič, Ľ. Structural, surface and magnetic properties of chalcogenide Co_9S_8 nanoparticles prepared by mechanochemical synthesis. *J. Alloy. Compd.* **2018**, *745*, 863–867. [CrossRef]
40. Patel, C.M.; Murthy, Z.V.P.; Chakraborty, M. Effects of operating parameters on the production of barium sulfate nanoparticles in stirred media mill. *J. Ind. Eng. Chem.* **2012**, *18*, 1450–1457. [CrossRef]
41. Patel, C.M.; Chakraborty, M.; Murthy, Z.V.P. Study on the stability and microstructural properties of barium sulfate nanoparticles produced by nanomilling. *Adv. Powder Technol.* **2014**, *25*, 226–235. [CrossRef]
42. Vicum, L.; Mazzotti, M.; Baldyga, J. Applying a thermodynamic model to the non-stoichiometric precipitation of barium sulfate. *Chem. Eng. Technol. Ind. Chem.-Plant Equip.-Process Eng.-Biotechnol.* **2003**, *26*, 325–333. [CrossRef]
43. Wojciechowski, K.; Kibalczyc, W. Light scattering study of KH_2PO_4 and $BaSO_4$ nucleation process. *J. Cryst. Growth* **1986**, *76*, 379–382. [CrossRef]
44. Bromley, L.A. Thermodynamic properties of strong electrolytes in aqueous solutions. *AIChE J.* **1973**, *19*, 313–320. [CrossRef]
45. Monnin, C. A thermodynamic model for the solubility of barite and celestite in electrolyte solutions and seawater to 200 °C and to 1 kbar. *Chem. Geol.* **1999**, *153*, 187–209. [CrossRef]
46. Leng, H.; Wang, X.; Niebur, G.L.; Roeder, R.K. Synthesis of a barium sulfate nanoparticle contrast agent for micro-computed tomography of bone microstructure. *Ceram. Nanomater. Nanotechnol. III* **2005**, *159*, 217–229.
47. Bala, H.; Fu, W.; Zhao, J.; Ding, X.; Jiang, Y.; Yu, K.; Wang, Z. Preparation of $BaSO_4$ nanoparticles with self-dispersing properties. *Colloids Surf. A Physicochem. Eng. Asp.* **2005**, *252*, 129–134. [CrossRef]
48. Sifontes, Á.B.; Cañizales, E.; Toro-Mendoza, J.; Ávila, E.; Hernández, P.; Delgado, B.A.; Cruz-Barrios, E. Obtaining highly crystalline barium sulphate nanoparticles via chemical precipitation and quenching in absence of polymer stabilizers. *J. Nanomater.* **2015**, *2015*, 6. [CrossRef]
49. Fang, C.; Hou, R.; Zhou, K.; Hua, F.; Cong, Y.; Zhang, J.; Cheng, Y.J. Surface functionalized barium sulfate nanoparticles: Controlled in situ synthesis and application in bone cement. *J. Mater. Chem. B* **2014**, *2*, 1264–1274. [CrossRef]
50. Bala, H.; Fu, W.; Guo, Y.; Zhao, J.; Jiang, Y.; Ding, X.; Wang, Z. In situ preparation and surface modification of barium sulfate nanoparticles. *Colloids Surf. A Physicochem. Eng. Asp.* **2006**, *274*, 71–76. [CrossRef]

51. Gupta, A.; Singh, P.; Shivakumara, C. Synthesis of $BaSO_4$ nanoparticles by precipitation method using sodium hexa metaphosphate as a stabilizer. *Solid State Commun.* **2010**, *150*, 386–388. [CrossRef]
52. Li, S.; Zheng, L.; Yu, L. Preparation of Flower-Shaped Barium Sulfate Nanoparticles in the Presence of DTAB. *J. Dispers. Sci. Technol.* **2011**, *32*, 601–603. [CrossRef]
53. Li, Y.; Wang, X.; Cui, Y.; Ma, W.; Guo, H. High dispersion barium sulfate nanoparticles prepared with dodecyl benzene sulfonic acid. *Int. J. Nanosci.* **2012**, *11*, 1240040. [CrossRef]
54. Ramaswamya, V.; Vimalathithan, R.M.; Ponnusamy, V. Synthesis of monodispersed barium sulphate nanoparticles using water-benzene mixed solvent. *Adv Mater Lett* **2012**, *3*, 29–33. [CrossRef]
55. Sokolova, V.; Loza, K.; Knuschke, T.; Heinen-Weiler, J.; Jastrow, H.; Hasenberg, M.; Epple, M. A systematic electron microscopic study on the uptake of barium sulphate nano-, submicro-, microparticles by bone marrow-derived phagocytosing cells. *Acta Biomater.* **2018**, *80*, 352–363. [CrossRef]
56. Prutviraj, K.; Ramesh, T.N. Surfactant mediated synthesis of barium sulfate, strontium sulfate and barium-strontium sulfate nanoparticles. *Inorg. Nano-Met. Chem.* **2019**, *49*, 93–99.
57. Shimpi, N.G.; Mishra, S. Ultrasonic-assisted synthesis of nano-$BaSO_4$ and its effect on thermal and cross-linking density of epoxy nanocomposites. *J. Reinf. Plast. Compos.* **2013**, *32*, 947–954. [CrossRef]
58. Jha, M.; Ansari, S.; Shimpi, N.G. Novel sonochemical green approach for synthesis of highly crystalline and thermally stable barium sulphate nanoparticles using Azadirachta indica leaf extract. *Bull. Mater. Sci.* **2019**, *42*, 22. [CrossRef]
59. Vidal-Vidal, J.; Rivas, J.; López-Quintela, M.A. Synthesis of monodisperse maghemite nanoparticles by the microemulsion method. *Colloids Surf. A Physicochem. Eng. Asp.* **2006**, *288*, 44–51. [CrossRef]
60. Solanki, J.N.; Sengupta, R.; Murthy, Z.V.P. Synthesis of copper sulphide and copper nanoparticles with microemulsion method. *Solid State Sci.* **2010**, *12*, 1560–1566. [CrossRef]
61. Yıldırım, Ö.A.; Durucan, C. Synthesis of zinc oxide nanoparticles elaborated by microemulsion method. *J. Alloy. Compd.* **2010**, *506*, 944–949. [CrossRef]
62. Bagwe, R.P.; Yang, C.; Hilliard, L.R.; Tan, W. Optimization of dye-doped silica nanoparticles prepared using a reverse microemulsion method. *Langmuir* **2004**, *20*, 8336–8342. [CrossRef] [PubMed]
63. Salabat, A.; Mirhoseini, F. A novel and simple microemulsion method for synthesis of biocompatible functionalized gold nanoparticles. *J. Mol. Liq.* **2018**, *268*, 849–853. [CrossRef]
64. Vafa, E.; Shahrokhi, M.; Molaei Dehkordi, A. Population Balance Modeling of Barium Sulfate Nanoparticle Synthesis via Inverse Microemulsion Including Coagulation Effect. *Ind. Eng. Chem. Res.* **2014**, *53*, 12705–12719. [CrossRef]
65. Gan, L.M.; Zhang, L.H.; Chan, H.S.O.; Chew, C.H. Preparation of conducting polyaniline-coated barium sulfate nanoparticles in inverse microemulsions. *Mater. Chem. Phys.* **1995**, *40*, 94–98. [CrossRef]
66. Qi, L.; Ma, J.; Cheng, H.; Zhao, Z. Preparation of $BaSO_4$ nanoparticles in non-ionic w/o microemulsions. *Colloids Surf. A Physicochem. Eng. Asp.* **1996**, *108*, 117–126. [CrossRef]
67. Hopwood, J.D.; Mann, S. Synthesis of barium sulfate nanoparticles and nanofilaments in reverse micelles and microemulsions. *Chem. Mater.* **1997**, *9*, 1819–1828. [CrossRef]
68. Ivanova, N.I.; Rudelev, D.S.; Summ, B.D.; Chalykh, A.A. Synthesis of barium sulfate nanoparticles in water-in-oil microemulsion systems. *Colloid J.* **2001**, *63*, 714–717. [CrossRef]
69. Adityawarman, D.; Voigt, A.; Veit, P.; Sundmacher, K. Precipitation of $BaSO_4$ nanoparticles in a non-ionic microemulsion: Identification of suitable control parameters. *Chem. Eng. Sci.* **2005**, *60*, 3373–3381. [CrossRef]
70. Ethayaraja, M.; Bandyopadhyaya, R. Population balance models and Monte Carlo simulation for nanoparticle formation in water-in-oil microemulsions: Implications for CdS synthesis. *J. Am. Chem. Soc.* **2006**, *128*, 17102–17113. [CrossRef]
71. Nourafkan, E.; Alamdari, A. Modeling of Silver Nanoparticle Synthesis in Ternary Reverse Microemulsion of Cyclohexane/Water/SDS. *Part. Sci. Technol.* **2014**, *32*, 215–223. [CrossRef]
72. Muralidharan, G.; Subramanian, L.; Nallamuthu, S.K.; Santhanam, V.; Kumar, S. Effect of reagent addition rate and temperature on synthesis of gold nanoparticles in microemulsion route. *Ind. Eng. Chem. Res.* **2011**, *50*, 8786–8791. [CrossRef]
73. Ramkrishna, D.; Mahoney, A.W. Population balance modeling. Promise for the future. *Chem. Eng. Sci.* **2002**, *57*, 595–606. [CrossRef]
74. Viswanadh, B.; Tikku, S.; Khilar, K.C. Modeling core–shell nanoparticle formation using three reactive microemulsions. *Colloids Surf. A Physicochem. Eng. Asp.* **2007**, *298*, 149–157. [CrossRef]
75. Liu, H.; Li, J.; Sun, D.; Odoom-Wubah, T.; Huang, J.; Li, Q. Modeling of silver nanoparticle formation in a microreactor: Reaction kinetics coupled with population balance model and fluid dynamics. *Ind. Eng. Chem. Res.* **2014**, *53*, 4263–4270. [CrossRef]
76. Niemann, B.; Rauscher, F.; Adityawarman, D.; Voigt, A.; Sundmacher, K. Microemulsion-assisted precipitation of particles: Experimental and model-based process analysis. *Chem. Eng. Processing Process Intensif.* **2006**, *45*, 917–935. [CrossRef]
77. Costa, C.B.B.; Maciel Filho, R. Nanoparticle processes modelling: The role of key parameters for population balances for on-line crystallization processes applications. *Powder Technol.* **2010**, *202*, 89–94. [CrossRef]
78. Niemann, B.; Sundmacher, K. Reduced discrete population balance model for precipitation of barium sulfate nanoparticles in non-ionic microemulsions. *Chem. Eng. J.* **2008**, *143*, 314–325. [CrossRef]
79. Bandyopadhyaya, R.; Kumar, R.; Gandhi, K.S. Modelling of $CaCO_3$ nanoparticle formation during overbasing of lubricating oil additives. *Langmuir* **2001**, *17*, 1015–1029. [CrossRef]

80. Bandyopadhyaya, R.; Kumar, R.; Gandhi, K.S. Simulation of precipitation reactions in reverse micelles. *Langmuir* **2000**, *16*, 7139–7149. [CrossRef]
81. Öncül, A.A.; Niemann, B.; Sundmacher, K.; Thévenin, D. CFD modelling of $BaSO_4$ precipitation inside microemulsion droplets in a semi-batch reactor. *Chem. Eng. J.* **2008**, *138*, 498–509. [CrossRef]
82. Niemann, B.; Veit, P.; Sundmacher, K. Nanoparticle precipitation in reverse microemulsions: Particle formation dynamics and tailoring of particle size distributions. *Langmuir* **2008**, *24*, 4320–4328. [CrossRef]
83. Köhler, J.M.; Abahmane, L.; Wagner, J.; Albert, J.; Mayer, G. Preparation of metal nanoparticles with varied composition for catalytical applications in microreactors. *Chem. Eng. Sci.* **2008**, *63*, 5048–5055. [CrossRef]
84. Rahman, M.; Rebrov, E.V. Microreactors for gold nanoparticles synthesis: From Faraday to flow. *Processes* **2014**, *2*, 466–493. [CrossRef]
85. Toyota, A.; Nakamura, H.; Ozono, H.; Yamashita, K.; Uehara, M.; Maeda, H. Combinatorial synthesis of CdSe nanoparticles using microreactors. *J. Phys. Chem. C* **2010**, *114*, 7527–7534. [CrossRef]
86. Simmons, M.; Wiles, C.; Rocher, V.; Francesconi, M.G.; Watts, P. The preparation of magnetic iron oxide nanoparticles in microreactors. *J. Flow Chem.* **2013**, *3*, 7–10. [CrossRef]
87. Abou-Hassan, A.; Neveu, S.; Dupuis, V.; Cabuil, V. Synthesis of cobalt ferrite nanoparticles in continuous-flow microreactors. *RSC Adv.* **2012**, *2*, 11263–11266. [CrossRef]
88. Wu, H.; Wang, C.; Zeng, C.; Zhang, L. Preparation of barium sulfate nanoparticles in an interdigital channel configuration micromixer SIMM-V2. *Ind. Eng. Chem. Res.* **2013**, *52*, 5313–5320. [CrossRef]
89. Kockmann, N.; Kastner, J.; Woias, P. Reactive particle precipitation in liquid microchannel flow. *Chem. Eng. J.* **2008**, *135*, S110–S116. [CrossRef]
90. Jeevarathinam, D.; Gupta, A.K.; Pitchumani, B.; Mohan, R. Effect of gas and liquid flowrates on the size distribution of barium sulfate nanoparticles precipitated in a two phase flow capillary microreactor. *Chem. Eng. J.* **2011**, *173*, 607–611. [CrossRef]
91. Su, Y.F.; Kim, H.; Kovenklioglu, S.; Lee, W.Y. Continuous nanoparticle production by microfluidic-based emulsion, mixing and crystallization. *J. Solid State Chem.* **2007**, *180*, 2625–2629. [CrossRef]
92. Schwarzer, H.C.; Peukert, W. Combined experimental/numerical study on the precipitation of nanoparticles. *AIChE J.* **2004**, *50*, 3234–3247. [CrossRef]
93. McCarthy, E.D.; Dunk, W.A.E.; Boodhoo, K.V.K. Application of an intensified narrow channel reactor to the aqueous phase precipitation of barium sulphate. *J. Colloid Interface Sci.* **2007**, *305*, 72–87. [CrossRef] [PubMed]
94. Kucher, M.; Babic, D.; Kind, M. Precipitation of barium sulfate: Experimental investigation about the influence of supersaturation and free lattice ion ratio on particle formation. *Chem. Eng. Processing Process Intensif.* **2006**, *45*, 900–907. [CrossRef]
95. Wang, Q.A.; Wang, J.X.; Li, M.; Shao, L.; Chen, J.F.; Gu, L.; An, Y.T. Large-scale preparation of barium sulphate nanoparticles in a high-throughput tube-in-tube microchannel reactor. *Chem. Eng. J.* **2009**, *149*, 473–478. [CrossRef]
96. Sen, N.; Koli, V.; Singh, K.K.; Panicker, L.; Sirsam, R.; Mukhopadhyay, S.; Shenoy, K.T. Segmented microfluidics for synthesis of $BaSO_4$ nanoparticles. *Chem. Eng. Processing-Process Intensif.* **2018**, *125*, 197–206. [CrossRef]
97. Pohl, B.; Jamshidi, R.; Brenner, G.; Peuker, U.A. Experimental study of continuous ultrasonic reactors for mixing and precipitation of nanoparticles. *Chem. Eng. Sci.* **2012**, *69*, 365–372. [CrossRef]
98. Hakke, V.; Sonawane, S.; Anandan, S.; Sonawane, S.; Ashokkumar, M. Process intensification approach using microreactors for synthesizing nanomaterials—A critical review. *Nanomaterials* **2021**, *11*, 98. [CrossRef]
99. Potapov, V.; Fediuk, R.; Gorev, D. Membrane concentration of hydrothermal SiO_2 nanoparticles. *Sep. Purif. Technol.* **2020**, *251*, 117290. [CrossRef]
100. Wang, Y.; Zhang, C.; Bi, S.; Luo, G. Preparation of ZnO nanoparticles using the direct precipitation method in a membrane dispersion micro-structured reactor. *Powder Technol.* **2010**, *202*, 130–136. [CrossRef]
101. Yang, L.; Guo, M.; Zhang, F.; Jing, Y.; Wang, Y.; Luo, G. Controllable preparation of γ-alumina nanoparticles with bimodal pore size distribution in membrane dispersion microreactor. *Particuology* **2018**, *41*, 1–10. [CrossRef]
102. Piacentini, E.; Poerio, T.; Bazzarelli, F.; Giorno, L. Continuous production of PVA-based hydrogel nanoparticles by membrane nanoprecipitation. *J. Membr. Sci.* **2021**, *637*, 119649. [CrossRef]
103. Chen, G.; Luo, G.; Xu, J.; Wang, J. Preparing ultrafine barium sulfate particles using membrane-dispersion-precipitation technology. *J.-Tsinghua Univ.* **2004**, *44*, 315–318.
104. Zhiqian, J.; Zhongzhou, L. Synthesis of nanosized $BaSO_4$ particles with a membrane reactor: Effects of operating parameters on particles. *J. Membr. Sci.* **2002**, *209*, 153–161. [CrossRef]
105. Chen, G.G.; Luo, G.S.; Xu, J.H.; Wang, J.D. Membrane dispersion precipitation method to prepare nanopartials. *Powder Technol.* **2004**, *139*, 180–185. [CrossRef]
106. Baker, R.W. Overview of membrane science and technology. *Membr. Technol. Appl.* **2004**, *3*, 1–14.
107. Chiavola, A.; Amato, E.D.; Stoller, M.; Chianese, A.; Boni, M.R. Application of iron based nanoparticles as adsorbents for arsenic removal from water. *Chem. Eng. Trans.* **2016**, *47*, 325–330.
108. Pask, S.D.; Nuyken, O.; Cai, Z. The spinning disk reactor: An example of a process intensification technology for polymers and particles. *Polym. Chem.* **2012**, *3*, 2698–2707. [CrossRef]
109. Tai, C.Y.; Wang, Y.H.; Liu, H.S. A green process for preparing silver nanoparticles using spinning disk reactor. *AIChE J.* **2008**, *54*, 445–452. [CrossRef]

110. Hartlieb, K.J.; Raston, C.L.; Saunders, M. Controlled scalable synthesis of ZnO nanoparticles. *Chem. Mater.* **2007**, *19*, 5453–5459. [CrossRef]
111. Chang, M.H.; Liu, H.S.; Tai, C.Y. Preparation of copper oxide nanoparticles and its application in nanofluid. *Powder Technol.* **2011**, *207*, 378–386. [CrossRef]
112. Mohammadi, S.; Harvey, A.; Boodhoo, K.V. Synthesis of TiO_2 nanoparticles in a spinning disc reactor. *Chem. Eng. J.* **2014**, *258*, 171–184. [CrossRef]
113. Cafiero, L.M.; Baffi, G.; Chianese, A.; Jachuck, R.J.J. Process intensification: Precipitation of barium sulfate using a spinning disk reactor. *Ind. Eng. Chem. Res.* **2002**, *41*, 5240–5246. [CrossRef]
114. Dehkordi, A.M.; Vafaeimanesh, A. Synthesis of barium sulfate nanoparticles using a spinning disk reactor: Effects of supersaturation, disk rotation speed, free ion ratio, and disk diameter. *Ind. Eng. Chem. Res.* **2009**, *48*, 7574–7580. [CrossRef]
115. Jacobsen, N.C.; Hinrichsen, O. Micromixing efficiency of a spinning disk reactor. *Ind. Eng. Chem. Res.* **2012**, *51*, 11643–11652. [CrossRef]
116. Farahani, H.B.; Shahrokhi, M.; Dehkordi, A.M. Experimental investigation and process intensification of barium sulfate nanoparticles synthesis via a new double coaxial spinning disks reactor. *Chem. Eng. Processing Process Intensif.* **2017**, *115*, 11–22. [CrossRef]
117. Jahanshahi-Anboohi, J.; Molaei Dehkordi, A. Continuous Synthesis of Barium Sulfate Nanoparticles in a New High-Speed Spinning Disk Reactor. *Ind. Eng. Chem. Res.* **2019**, *58*, 16597–16609. [CrossRef]
118. Meeuwse, M.; van der Schaaf, J.; Schouten, J.C. Multistage rotor-stator spinning disc reactor. *AIChE J.* **2012**, *58*, 247–255. [CrossRef]